# Chimera states in nonlocal phase-coupled oscillators

Edgar Knobloch

University of California at Berkeley

*knobloch@berkeley.edu*

7 May, 2019

http://tardis.berkeley.edu

Joint with J. Xie, H.-C. Kao, O. Omel'chenko, M. Wolfrum

Workshop on Patterns of Synchrony: Chimera States and Beyond
ICTP, Trieste

# Coupled oscillator systems

Examples of model equations:

**Complex Ginzburg-Landau equation**

$$A_t = A + (1 + i\alpha)\nabla^2 A - (1 + i\beta)|A|^2 A$$

**Reaction-diffusion equations**

$$u_t = Du_{xx} + R(u)$$

**Excitable systems: Fitzhugh-Nagumo equation**

$$u_t = u_{xx} + u(u - a)(1 - u) + v, \quad v_t = u - v$$

All these dynamical systems produce periodic structures which can be regarded as oscillators.

# Phase-coupled oscillator systems

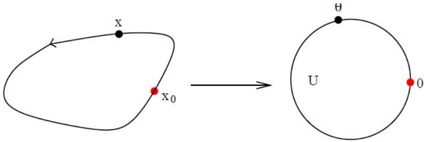


## One-oscillator problem

$$\frac{dX}{dt} = F(X)$$

Suppose $X_0(t) = X_0(t+T)$ is a stable periodic solution. We may associate a phase $\theta$ with points on $X_0$ so that

$$\frac{d\theta(X)}{dt} = \omega$$

# Phase-coupled oscillator systems

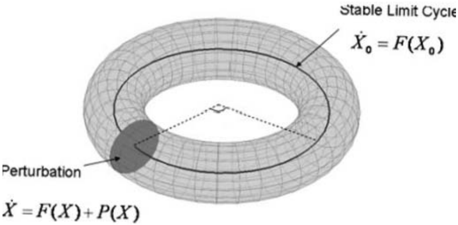


## Multi-oscillator problem

$$\frac{dX_i}{dt} = F_i(X_i) + \epsilon p_i(X_1, \cdots, X_i, \cdots)$$

The equations can be approximated as

$$\frac{d\theta_i}{dt} = \omega_i + \sum_j \Gamma_{ij}(\theta_i - \theta_j)$$

# Kuramoto model

## Kuramoto model (1975)

Assume $\Gamma_{ij}(\theta_i - \theta_j) = -\frac{K}{N}\sin(\theta_i - \theta_j)$,

$$\frac{d\theta_i}{dt} = \omega_i - \frac{K}{N}\sum_{j=1}^{N}\sin(\theta_i - \theta_j)$$

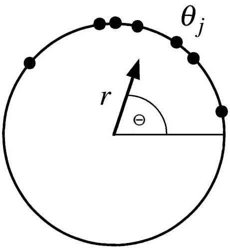


Kuramoto order parameter

$$r\exp(i\Theta) = \frac{1}{N}\sum_{j}^{N}\exp(i\theta_j)$$

# Kuramoto model

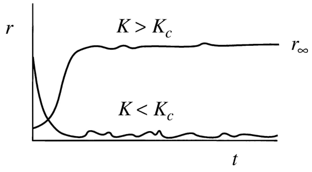


Figure: Asymptotic behavior

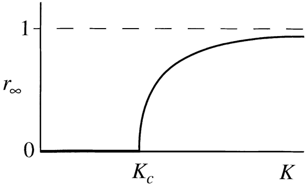


Figure: Bifurcation diagram

## Important quantities

- unimodal frequency distribution $g(\omega)$
- critical coupling constant $K_c = \frac{2}{\pi g(0)}$

# Chimera states: identical oscillators

We consider a system of nonlocal phase oscillators on a ring:

$$\frac{\partial \theta}{\partial t} = \omega - \int G(x-y)\sin[\theta(x,t) - \theta(y,t) + \alpha]dy$$

Here

$\theta$: phase variable
$G$: coupling function
$\omega$: natural frequencies
$\alpha$: phase lag ($\beta = \frac{\pi}{2} - \alpha$)

Chimera states: discovered by Kuramoto & Battogtokh (2002), and named "chimera states" by Abrams and Strogatz (2004)

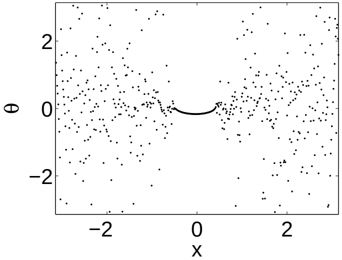


Figure: A snapshot of the phase distribution in a chimera state.

# Properties of the interaction kernel

## Which non-local coupling yields chimera?

- $G(x) = \exp(-\kappa|x|)$
- $G(x) = \begin{cases} \frac{1}{2r}, & |x| < r \\ 0, & otherwise \end{cases}$
- $G(x) = 1 + \gamma \cos(x), \quad \gamma < 1$
- $\cdots$

## Basic properties

$G(x) = G(-x)$, non-negative, non-increasing with $|x|$

Are these properties necessary? What happens if not all these conditions are satisfied?

## Repulsive coupling

- $G_n^{(1)}(x) = \cos(nx)$
- $G_n^{(2)}(x) = \cos(nx) + \gamma \cos[(n+1)x], \quad \gamma > \gamma_c$

# Properties of the interaction kernel: $\gamma = 1$

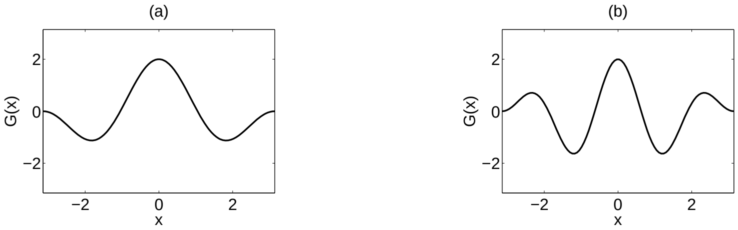


$G_1^{(2)}(x) = \cos(x) + \cos(2x)$

$G_2^{(2)}(x) = \cos(2x) + \cos(3x)$

# Theory

We define a local mean field $z(x,t)$ as the local average of $\exp[i\theta(x,t)]$,

$$z(x,t) \equiv \lim_{\delta \to 0^+} \frac{1}{\delta} \int_{-\delta/2}^{\delta/2} e^{i\theta(x+y,t)}\, dy.$$

The evolution equation for $z$ then takes the form (Pikovsky & Rosenblum, PRL **101**, 264103 (2008); Wolfrum *et al.*, Chaos **21**, 013112 (2011))

$$z_t = \frac{1}{2}\left(e^{-i\alpha} Z - e^{i\alpha} z^2 Z^*\right),$$

where $Z(x,t) \equiv K[z](x,t)$ and $K$ is a compact linear operator defined via the relation

$$K[z](x,t) \equiv \int_{-\pi}^{\pi} G(x-y) z(y,t)\, dy.$$

Stationary rotating solutions have the form $z(x,t) = \tilde{z}(x) e^{-i\Omega t}$, whose common frequency $\Omega$ satisfies the nonlinear eigenvalue relation

$$i\Omega\tilde{z} + \frac{1}{2}\left[e^{-i\alpha}\tilde{Z}(x) - e^{i\alpha}\tilde{z}^2\tilde{Z}^*(x)\right] = 0.$$

# Theory

Solving this equation as a quadratic equation in $\tilde{z}$ we obtain

$$\tilde{z}(x) = e^{i\beta} \frac{\Omega - \mu(x)}{\tilde{Z}^*(x)} = \frac{e^{i\beta} \tilde{Z}(x)}{\Omega + \mu(x)}.$$

The function $\mu$ is chosen to be $(\Omega^2 - |\tilde{Z}|^2)^{1/2}$ when $|\Omega| > |\tilde{Z}|$ and $i(|\tilde{Z}|^2 - \Omega^2)^{1/2}$ when $|\Omega| < |\tilde{Z}|$. It follows that:

$$\tilde{Z}(x) \equiv R(x) e^{i\Theta(x)} = e^{i\beta} \left\langle G(x-y) \frac{\Omega - \mu(y)}{\tilde{Z}^*(y)} \right\rangle.$$

We refer to $R(x)$ and $\Theta(x)$ as the amplitude and phase of the complex order parameter $\tilde{Z}(x)$. This equation can be also obtained from the Ott-Antonsen Ansatz (2008). The resulting **self-consistency** relation forms the basis for the theory that follows.

# The coupling: $G_1^{(1)}(x) = \cos(x)$

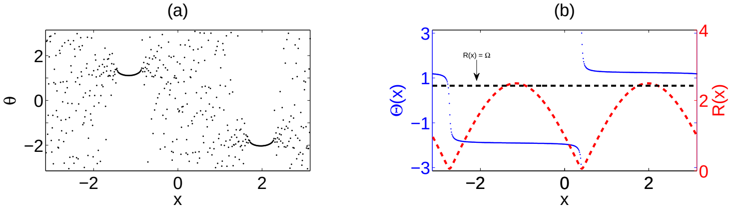


Figure: (a) The phase distribution $\theta$ in a chimera state with coupling $G_1^{(1)}(x) \equiv \cos(x)$ when $\beta = 0.1$ and $N = 512$. (b) The local order parameters $R$ (red dashed line) and $\Theta$ (blue dotted line).

## Self-consistency equation

$$R_0^2 = \exp(i\beta) \left\langle \Omega - \sqrt{\Omega^2 - R_0^2 \cos^2(x)} \right\rangle$$

# Dependence on $\beta$

The boundary of the coherent fraction is determined by $|R_0 \cos(x)| = \Omega$, so that the coherent fraction is given by $e = 2\cos^{-1}(\Omega/R_0)/\pi$

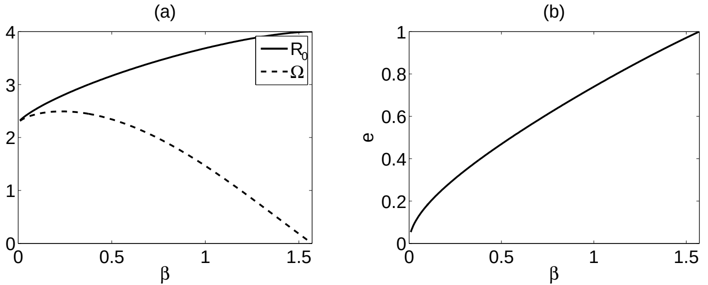


Figure: (a) The quantities $R_0$ and $\Omega$, and (b) the coherent fraction $e$, all as functions of $\beta$ for the 2-cluster chimera state with $G_1^{(1)}(x)$ coupling.

# Stability

The evolution equation for an infinitesimal perturbation $v$ of $\tilde{z}(x)$ is

$$v_t = i\mu v + \frac{1}{2}\left[e^{-i\alpha}V - \tilde{z}^2 e^{i\alpha}V^*\right],$$

where $V(x,t) \equiv Kv(x,t)$. Solutions of this nonlocal problem are of the form $v(x,t) = e^{\lambda t}v_1(x) + e^{\lambda^* t}v_2^*(x)$, where $\lambda$ is the growth rate:

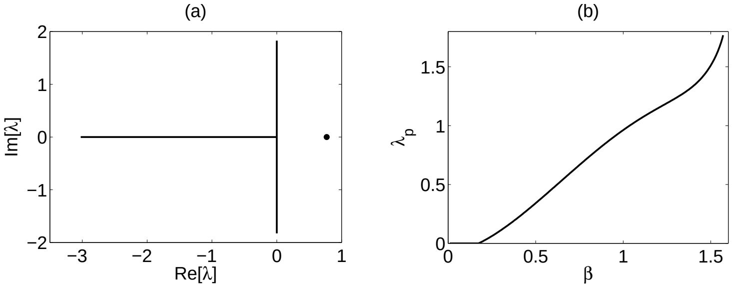


Figure: (a) Spectrum of the linearized operator about 2-cluster chimera state for $G_1^{(1)}$ when $\beta \approx 0.83$. (b) Dependence of the point eigenvalue $\lambda_p$ on $\beta$; the state loses stability at $\beta \approx 0.17$.

# The coupling: $G_1^{(2)}(x) \equiv \cos(x) + \cos(2x)$

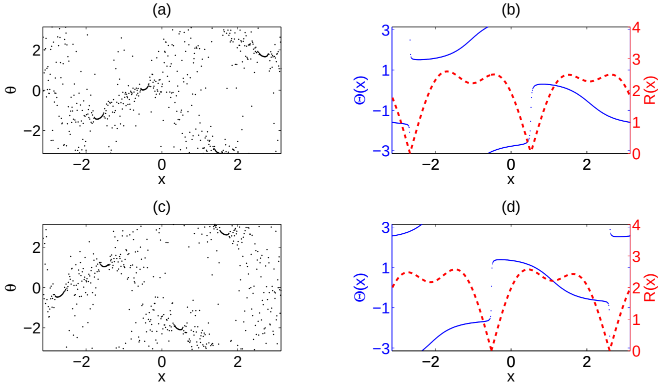


Figure: (a) The phase distribution $\theta(x)$ in a 4-cluster chimera state with coupling $G_1^{(2)} \equiv \cos(x) + \cos(2x)$ and $\beta = 0.03$, $N = 512$. (b) The local order parameters $R$ (red dashed line) and $\Theta$ (blue dotted line). (c,d) A related chimera state with order parameters $R$ and $-\Theta$.

# The coupling: $G_1^{(2)}(x) \equiv \cos(x) + \cos(2x)$

When $\beta$ increases to a certain threshold, coherent clusters merge.

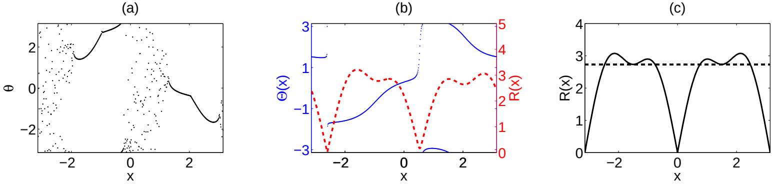


Figure: (a) The computed phase distribution $\theta(x)$ at $\beta = 0.24$. (b) The corresponding order parameter $R(x)$ (red dashed line) and associated phase $\Theta(x)$ (blue dotted line). (c) The order parameter $R(x)$ and $\Omega$.

# Traveling coherent states with $G_1^{(2)}$ coupling

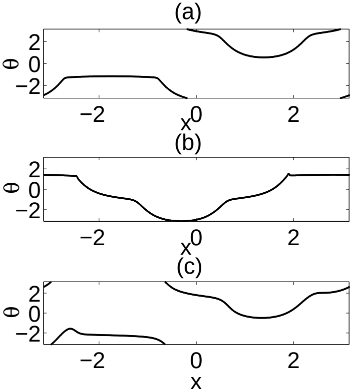


Figure: (a) The phase distribution $\theta(x)$ at (a) $\beta = 0.77$ (symmetric distribution), (b) $\beta = 0.76$ (asymmetric distribution) and (c) $\beta = 0.66$ (asymmetric distribution), all for $N = 512$. The state in (b) oscillates in time while drifting to the left; state (c) travels to the left at constant speed. Reflected solutions travel to the right.

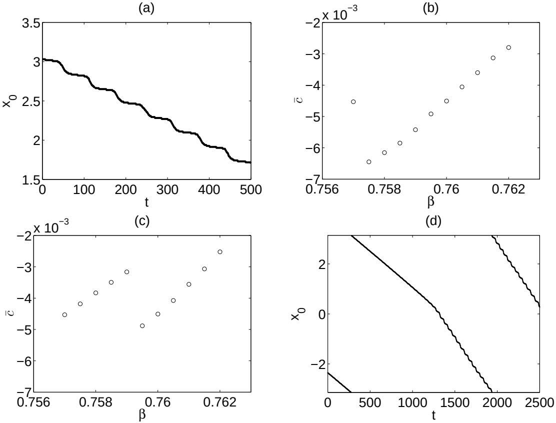


Figure: (a) The position $x_0$ of the coherent state as a function of time (mod $2\pi$) at $\beta = 0.762$. (b) The time-averaged speed $\bar{c}$ of the coherent state as a function of $\beta$ as $\beta$ decreases. Note the abrupt decrease in speed at $\beta \approx 0.7570$ associated with the disappearance of the oscillations. (c) The time-averaged speed $\bar{c}$ of the coherent state as a function of $\beta$ as $\beta$ increases. Oscillations reappear at $\beta \approx 0.7595$ as shown in (d). All calculations are for $N = 512$.

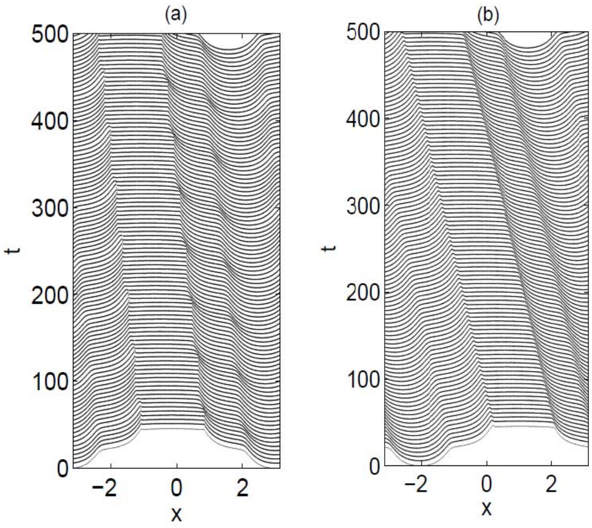


Figure: Hidden line plots of the phase distribution $\theta$ as a function of time when (a) $\beta = 0.762$ (oscillatory drift) and (b) $\beta = 0.755$ (constant drift), both for $N = 512$.

We suppose that $z(x,t) \equiv u(\xi)$, where $\xi \equiv x - ct$, obtaining a complex nonlinear eigenvalue problem for the speed $c$ and the frequency $\Omega$ of the coherent state:

$$c\tilde{u}_\xi + i\Omega\tilde{u} + \frac{1}{2}\left[e^{-i\alpha}\tilde{U} - \tilde{u}^2 e^{i\alpha}\tilde{U}^*\right] = 0,$$

where $\tilde{u} = u \exp i\Omega t$ and likewise for $\tilde{U}$.

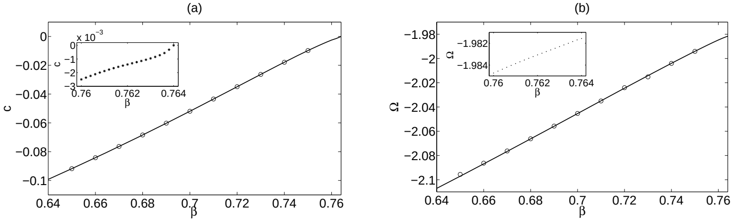


Figure: Comparison of (a) the speed $c$ and (b) the frequency $\Omega$ obtained from the solution of the nonlinear eigenvalue problem (solid lines) with measurements computed with $N = 512$ oscillators (open circles), both as a function of $\beta$. The inset in (a) reveals the expected square root behavior near $\beta_c \approx 0.7644$. In contrast, the behavior of $\Omega$ is approximately linear everywhere.

# Traveling chimera states with $G_3^{(2)}$ coupling

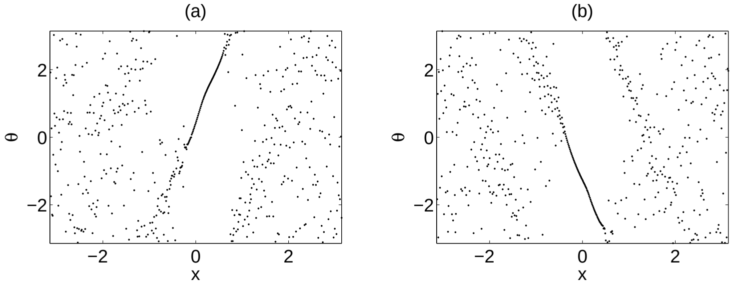


Figure: (a) A left-traveling 1-cluster chimera state. (b) A right-traveling 1-cluster chimera state. The simulation is done for $\beta = 0.03$ with the coupling $G_3^{(2)} \equiv \cos(3x) + \cos(4x)$ and $N = 512$.

Traveling chimeras generated by **asymmetric** coupling are studied by Omel'chenko (2019)

# Traveling chimera states with $G_3^{(2)}$ coupling

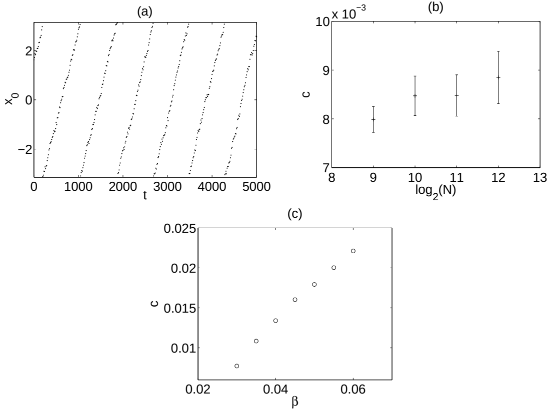


Figure: (a) The position $x_0$ of the coherent cluster as a function of time when $N = 512$, $\beta = 0.03$. (b) The dependence of the speed $c$ of the cluster on the oscillator number $N$ when $\beta = 0.03$. (c) The dependence of the speed $c$ of the cluster on the parameter $\beta$ when $N = 512$.

# Traveling chimera states with $G_3^{(2)}$ coupling

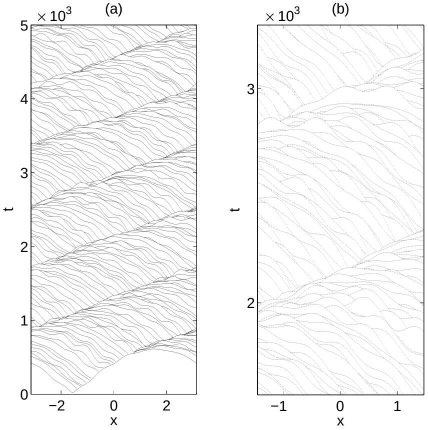


Figure: (a) The local order parameter $R(x,t)$ in a space-time plot for the traveling chimera. (b) Zoom of (a) showing additional detail.

# Effect of inhomogeneity in the natural frequencies

## Model equation

$$\frac{\partial \theta}{\partial t} = \omega(x) - \int G(x-y)\sin[\theta(x,t) - \theta(y,t) + \alpha]dy$$

## Effect of $\omega(x)$

- Break-up splay states
- Pin the chimera states to specific locations
- Trap traveling chimeras

# Effect on traveling coherent states: $\omega(x) = \omega_0 \exp(-\kappa|x|)$

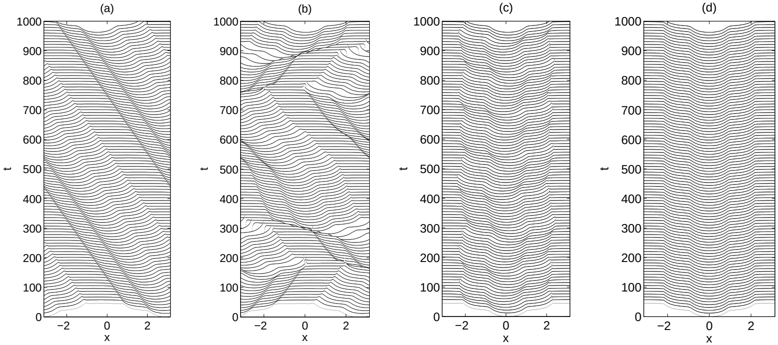


Figure: Hidden line plot of the phase distribution $\theta(x,t)$ when (a) $\omega_0 = 0$. (b) $\omega_0 = 0.04$. (c) $\omega_0 = 0.08$. (d) $\omega_0 = 0.12$. In all cases, $\kappa = 2$, $\beta = 0.75$ and $N = 512$.

# Hysteresis: $\omega(x) = \omega_0 \exp(-\kappa|x|)$

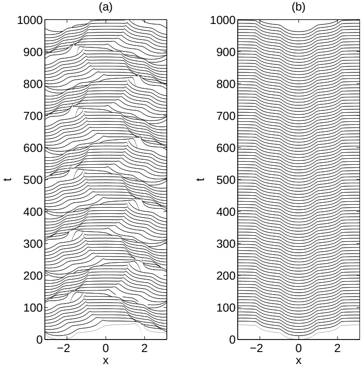


Figure: Hidden line plot of the $\theta(x,t)$ when $\omega_0 = 0.12$ and $\beta = 0.76$. (a) Unpinned state obtained from a traveling coherent state with $\omega_0 = 0$ and $\beta = 0.76$ on gradually increasing $\omega_0$ to 0.12. (b) Pinned state obtained from a traveling coherent with $\omega_0 = 0$ and $\beta = 0.75$ on gradually increasing $\omega_0$ to 0.12, and then increasing $\beta$ to 0.76. In both cases $\kappa = 2$ and $N = 512$.

# Effect on traveling chimera states: $\omega(x) = \omega_0 \exp(-\kappa|x|)$

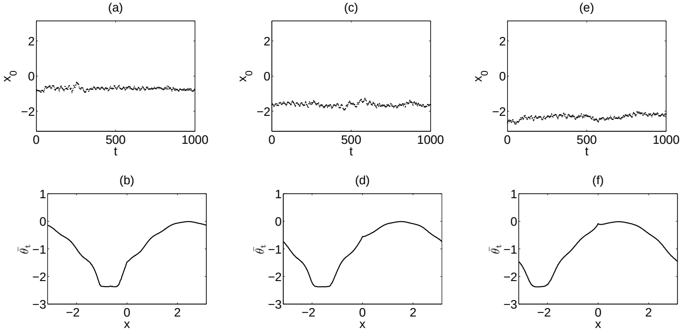


Figure: The position $x_0$ of the pinned coherent cluster in a traveling chimera state as a function of time when (a) $\omega_0 = 0.04$, (c) $\omega_0 = 0.08$, (e) $\omega_0 = 0.12$. The average rotation frequency $\bar{\theta}_t$ for (b) $\omega_0 = 0.04$, (d) $\omega_0 = 0.08$, (f) $\omega_0 = 0.12$. In all cases $\beta = 0.03$ and $\kappa = 10$, $N = 512$.

The location of the trapped coherent cluster moves further from $x = 0$ as $\omega_0$ increases.

# Two-dimensional systems

## Model equation

$$\frac{\partial\theta(x,y,t)}{\partial t} = -\int_{-\pi}^{\pi}\int_{-\pi}^{\pi} G\left(x-x', y-y'\right)\sin(\theta(x,y,t)-\theta(x',y',t)+\alpha)\,dx'\,dy'$$

## Coupling choice

We assume $G$ can be decomposed as $G(x,y) = G_x(x) + G_y(y)$, with $G_x$ and $G_y$ chosen from the following two families:

$$G_n^{(1)}(x) \equiv \cos(nx), \quad G_n^{(2)}(x) \equiv \cos(nx) + \gamma\cos[(n+1)x].$$

## Two properties

1. The system is invariant under the group $D_4$.
2. If $\theta_1(x,t)$ is a solution for the one-dimensional system

$$\frac{\partial\theta(x,t)}{\partial t} = -\int_{-\pi}^{\pi} G(x-x')\sin[\theta(x,t)-\theta(x',t)+\alpha]\,dx',$$

then $\theta_2(x,y,t) \equiv \theta_1(x, 2\pi t)$ is a solution of corresponding 2D system.

# Traveling coherent states and traveling chimera states

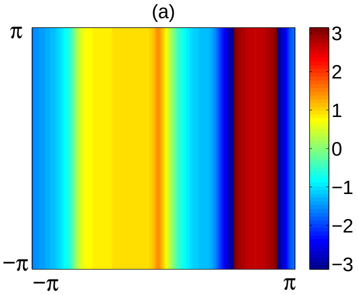


Figure: (a) Snapshot of the phase pattern in a right-traveling coherent state. The simulation is done for $G_x = G_y = G_1^{(2)}$, with $\beta = 0.7$ and $N = 256$. (b) Snapshot of the phase pattern for a right-traveling chimera state. The simulation is done for $G_x = G_y = G_3^{(2)}$, with $\beta = 0.03$ and $N = 256$.

# 1:1 twisted chimera state for $G_x = G_y = G_1^{(1)}$

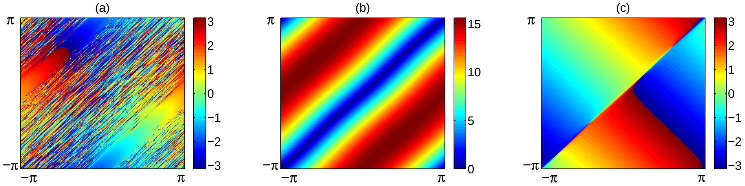


Figure: Snapshot of the phase pattern for the 1:1 twisted chimera state. (a) The phase distribution $\theta(x, y)$. (b) The corresponding order parameter $R(x, y)$. (c) The corresponding order parameter $\Theta(x, y)$, all for $G_x = \cos(x)$, $G_y = \cos(y)$, $\beta = 0.05$, $N = 256$ from a random initial condition. In panels (a) and (c), the color indicates the phase of the oscillators; in (b), the color indicates the amplitude of the local order parameter $R(x, y)$.

# 1:2 twisted chimera state for $G_x = G_y = G_1^{(2)}$

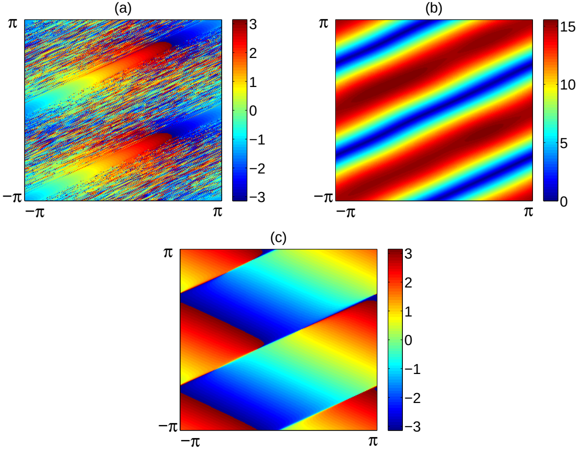


Figure: (a) Snapshot of the phase distribution in a 1:2 chimera state. (b) The corresponding order parameter $R$. (c) The corresponding order parameter $\Theta$. The simulation is done for $G_x = G_y = G_1^{(2)}$, with $\beta = 0.05$, $N = 256$.

# Multi-core spiral wave chimera states

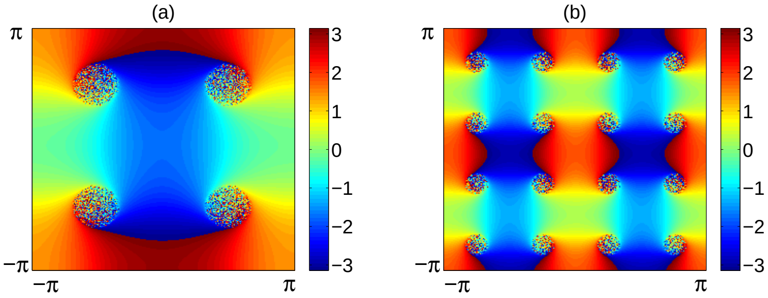


Figure: Snapshots of the phase pattern for spiral wave chimera states. (a) The phase distribution $\theta(x, y)$ for $G_x = G_y = G_1^{(1)}$. (b) The phase distribution $\theta(x, y)$ for $G_x = G_y = G_2^{(1)}$. The upper left spirals rotate clockwise in both (a) and (b), with the direction of rotation alternating from core to core in both $x$ and $y$ directions. The phase patterns have the symmetry $D_2$ and not $D_4$. Simulations are done with $\beta = 1$, $N = 256$ and random initial condition.

# Multi-core spiral wave chimera states

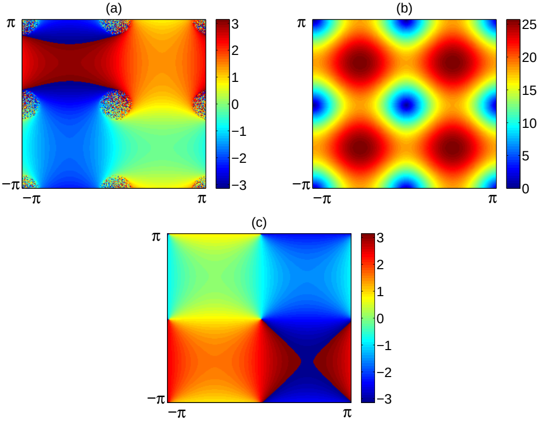


Figure: (a) Snapshot of the phase distribution $\theta(x, y)$ for a four-core spiral wave chimera state for $\beta = 1$ after translation of one of the incoherent cores to the origin. (b) Corresponding order parameter $R(x, y)$. (c) Corresponding order parameter $\Theta(x, y)$. The simulation is done with $G_x = G_y = G_1^{(1)}$, $N = 256$ and random initial condition.

# Multi-core spiral wave chimera states

The order parameter takes the form $R\exp(i\Theta) = b(\sin x + i \sin y)$, and the self-consistency equation is

$$2b^2 = \exp(i\beta)\left\langle \Omega - \sqrt{\Omega^2 - b^2(\sin^2 x + \sin^2 y)} \right\rangle .$$

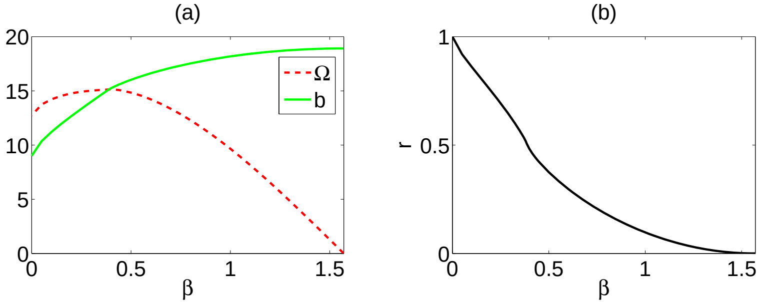


Figure: Dependence on the parameter $\beta$ of (a) $b$, $\Omega$, and (b) the fraction $r$ of incoherent oscillators. When $\Omega = b$, incoherent cores touch each other, as shown in the following slide.

# Multi-core spiral wave chimera states

As $\beta$ decreases to a threshold $\beta = \beta_c \approx 0.38$, the incoherent domains reconnect and the coherent domains separate into four isolated islands.

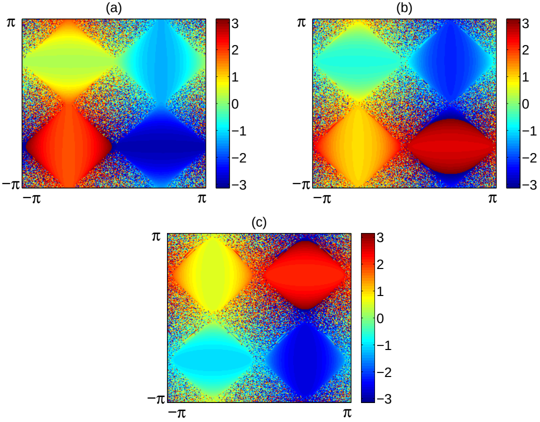


Figure: Snapshots of the phase patterns for spiral wave chimeras showing localized regions of coherence embedded in an incoherent background. (a) $\beta = 0.4$. (b) $\beta = 0.38$. (c) $\beta = 0.36$. Here $G_x = G_y = G_1^{(1)}$, $N = 256$.

# Exotic spiral wave chimera states

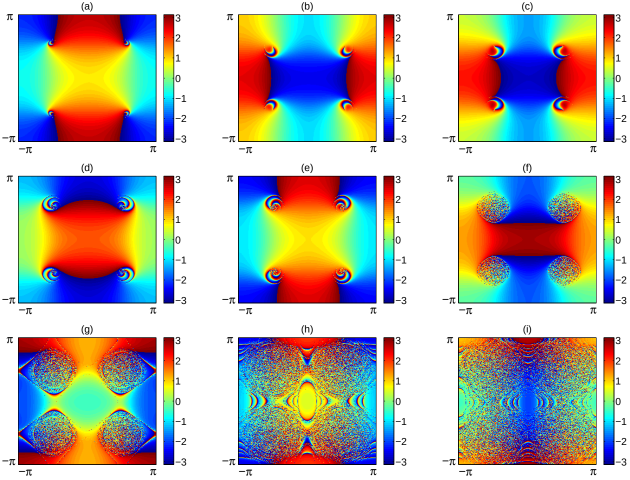


Figure: Snapshots of chimera states for $G_x = G_y = G_1^{(2)}$, $N = 256$, obtained by gradually decreasing $\beta$: (a) $\beta = 1.4$. (b) $\beta = 1.2$. (c) $\beta = 1.118$. (d) $\beta = 1.117$. (e) $\beta = 1.1$. (f) $\beta = 0.8$. (g) $\beta = 0.4$. (h) $\beta = 0.06$. (i) $\beta = 0.025$.

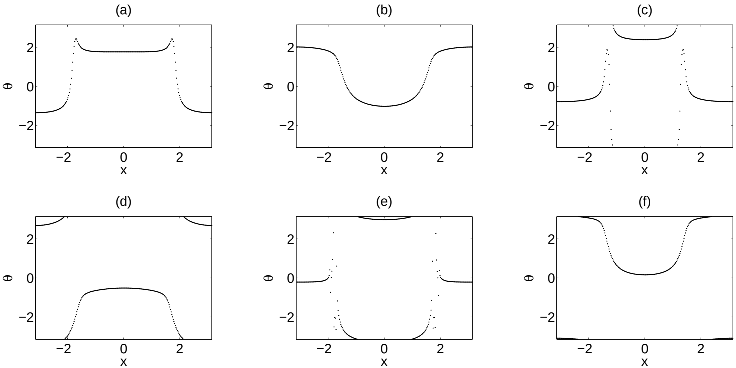


Figure: Snapshots of the phase pattern $\theta(x, y_0, t)$ for $G_x = G_y = G_1^{(2)}$, with $N = 256$ and $\beta = 1.4$: (a) $t = 0$, (b) $t = 5$, (c) $t = 10$, (d) $t = 15$, (e) $t = 20$, (f) $t = 25$, corresponding to a slice through the upper two cores of (a) of the previous figure. Note the significant detraining of some oscillators in panels (c) and (e).

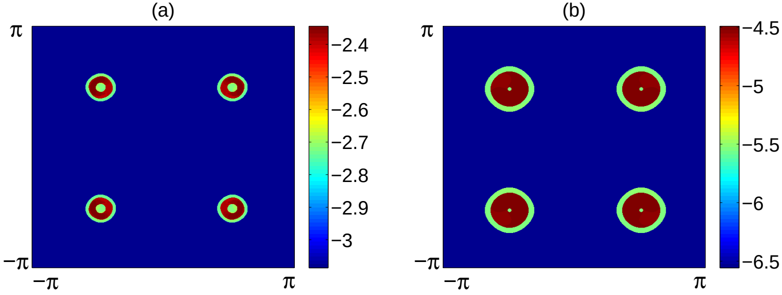


Figure: Snapshots of the oscillator frequency $\bar{\theta}_t(x,y)$ averaged over the time interval $0 \le t \le 250$ for $G_x = G_y = G_1^{(2)}$ and $N = 512$. (a) $\beta = 1.4$, (b) $\beta = 1.2$. These figures confirm the presence of a nonmonotonic frequency profile in the partially incoherent core when $\beta = 1.4$ as also obtained with $N = 256$ oscillators.

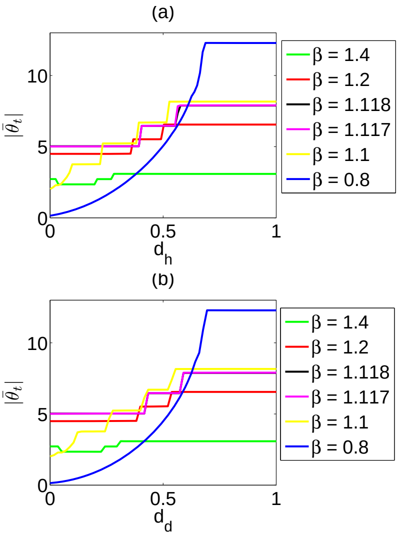


Figure: The mean oscillation frequency $\bar{\theta}_t$ as a function of (a) the horizontal distance $d_h$, (b) the diagonal distance $d_d$ from the center of a core for different values of $\beta$, showing a stepwise but monotonic dependence for $0.8 \lesssim \beta \lesssim 1.2$ and a stepwise nonmonotonic dependence for $\beta = 1.4$.

# Stability of 4-core and 16-core chimeras

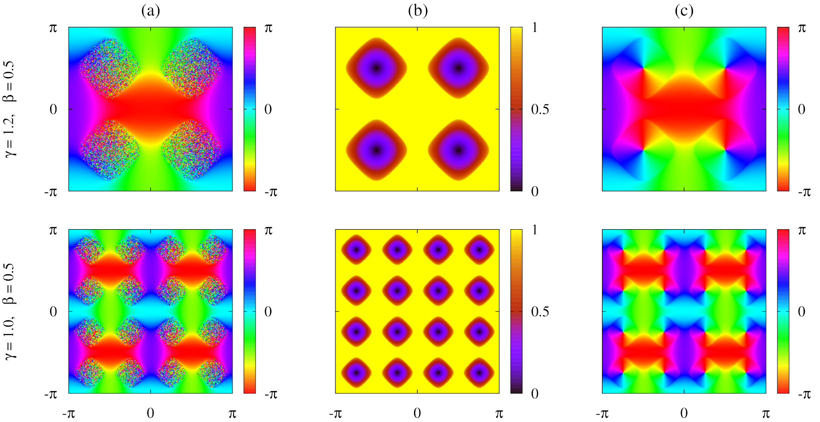


Four-core (upper row) and 16-core (lower row) spiral chimeras. (a) Phase snapshots, (b) modulus and (c) argument of the complex order parameter $a(x, y)$ at a particular instant in time.

$$4 - \text{core} : w(x, y) = p(\cos x + i \cos y), \quad 16 - \text{core} : w(x, y) = p(\cos 2x + i \cos 2y)$$

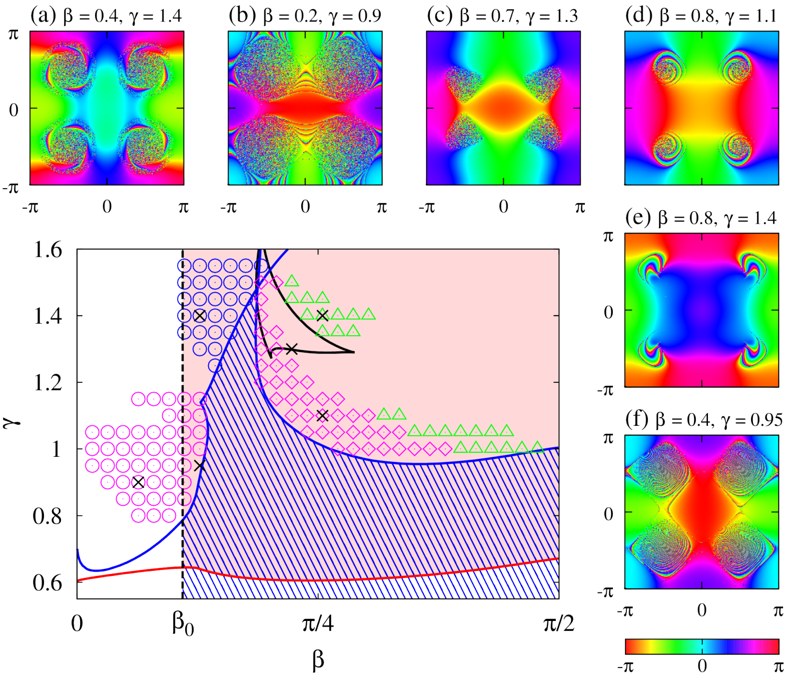

(a) β = 0.4, γ = 1.4
(b) β = 0.2, γ = 0.9
(c) β = 0.7, γ = 1.3
(d) β = 0.8, γ = 1.1
(e) β = 0.8, γ = 1.4
(f) β = 0.4, γ = 0.95
π
0
-π
γ
β
1.6
1.4
1.2
1
0.8
0.6
0
β0
π/4
π/2

# Linear stability problem for the 4-core spiral state

We write the perturbation in the form

$$v(x,y,t) = v_+(x,y)e^{\lambda t} + \overline{v}_-(x,y)e^{\overline{\lambda}t}$$

and find that $\lambda$ solves the eigenvalue problem

$$\begin{pmatrix} v_+ \\ v_- \end{pmatrix} = \frac{1}{2}\begin{pmatrix} e^{-i\alpha}\left(\lambda + \Omega\eta(|w|^2)\right)^{-1}\left(\mathcal{G}v_+ + a^2\mathcal{G}v_-\right) \\ e^{i\alpha}\left(\lambda + \Omega\overline{\eta(|w|^2)}\right)^{-1}\left(\mathcal{G}v_- + \overline{a}^2\mathcal{G}v_+\right) \end{pmatrix},$$

where $(\mathcal{G}\varphi)(x,y) := \int_{-\pi}^{\pi} dx' \int_{-\pi}^{\pi} G(x-x', y-y')\varphi(x',y')dy'$.

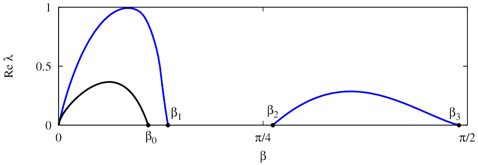


Figure: Unstable real eigenvalue (black curve) and the real part of the unstable complex eigenvalues (blue curve) for $\gamma = 1$. Bifurcation points: $\beta_0 \approx 0.34$, $\beta_1 \approx 0.42$, $\beta_2 \approx 0.82$ and $\beta_3 \approx 1.54$.

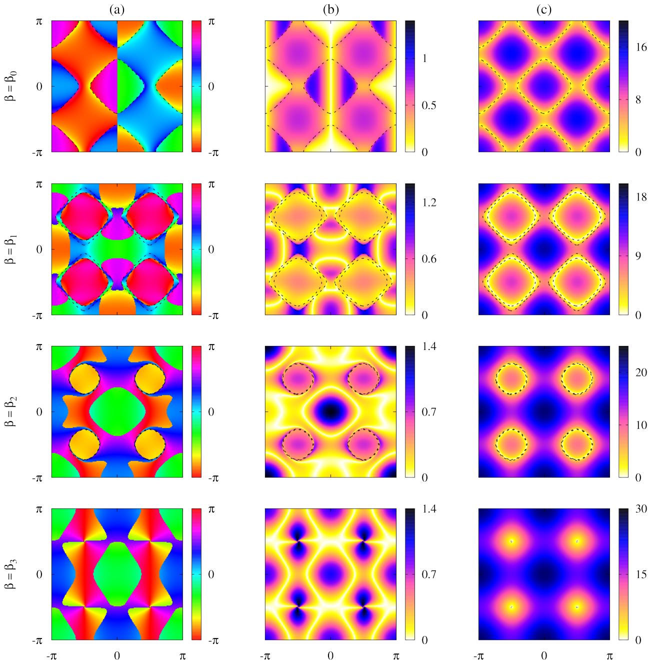

(a)
(b)
(c)
β = β0
β = β1
β = β2
β = β3
π
0
-π
1
0.5
16
8
1.2
0.6
18
9
1.4
0.7
20
10
30
15

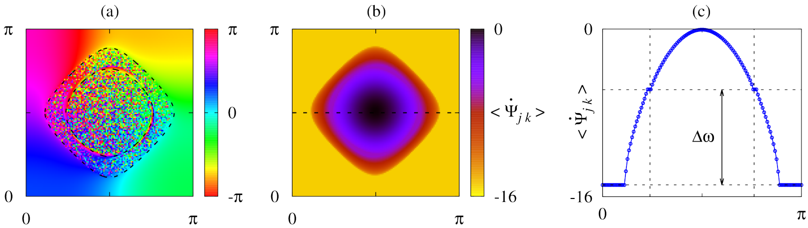


Figure: (a) Snapshot of the top-right core of the symmetric four-core spiral chimera pattern to the left of the left Hopf bifurcation. (b) Mean phase velocities and (c) a one-dimensional section corresponding to the dashed line in panel (b). Parameters: $N = 256$, $\gamma = 1.3$ and $\beta = 0.475$. The two dashed curves in panel (a) show the coherence-incoherence boundary

$$\cos^2 x + \cos^2 y = p^{-2}$$

and the singularity curve

$$\cos^2 x + \cos^2 y = p^{-2}\left(1 - (\omega_{\mathrm{cr}}/\Omega_p)^2\right)$$

for $\beta = 0.483$, the value of $\beta$ corresponding to the left Hopf bifurcation when $\gamma = 1.3$. Vertical dashed lines in panel (c) denote position of the singularity curve for $\beta = 0.483$. Horizontal dashed curves in panel (c) show the frequency-locking plateaus in the two coherent regions.

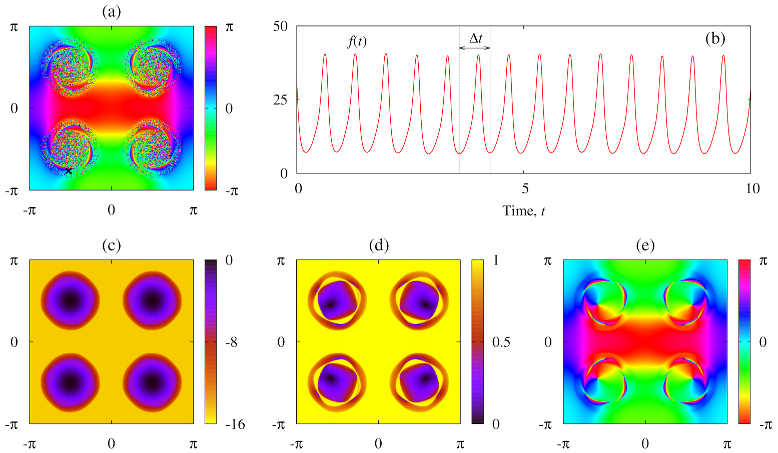


Figure: (a) Snapshot of a quasiperiodic spiral chimera for $N = 256$, $\gamma = 1.4$ and $\beta = 0.45$. (b) The indicator function $f(t) \equiv (2\pi/N)^{-1} \sin(\Psi_{mn}(t) - \Psi_{m\,n-1}(t))$ for $(m, n) = (61, 30)$ (cross in panel (a)) showing periodic modulation with new period $\Delta t$, where $\Delta t$ is the time interval between consecutive minima. (c) Mean phase velocities. (d) Modulus and (e) argument of the local order parameter $Z_{jk}$.

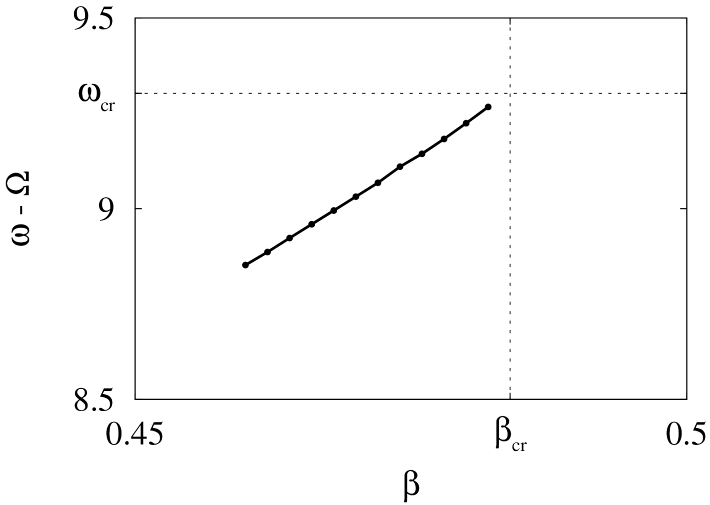


Figure: Difference between the secondary frequency $\omega$ and the collective frequency $\Omega$ for different $\beta$. Parameters: $N = 256$ and $\gamma = 1.3$.

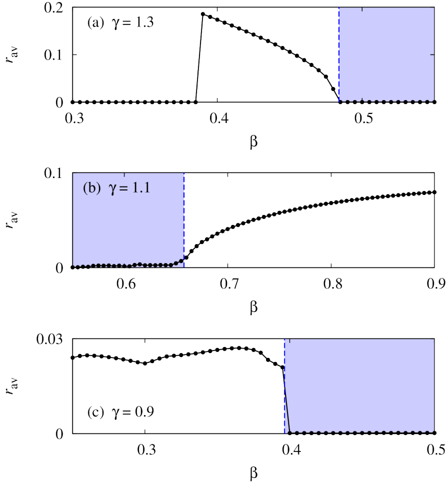


Figure: Time-averaged Kuramoto order parameter $r(t) = |\frac{1}{N^2}\sum_{m,n=1}^{N} e^{i\Psi_{mn}(t)}|$ for spatiotemporal patterns with $N = 1024$. (a) $\gamma = 1.3$ and $\beta$ decreasing from 0.55 to 0.3, (b) $\gamma = 1.1$ and $\beta$ increasing from 0.55 to 0.9, (c) $\gamma = 0.9$ and $\beta$ decreasing from 0.5 to 0.25. Blue shaded regions show stability intervals.

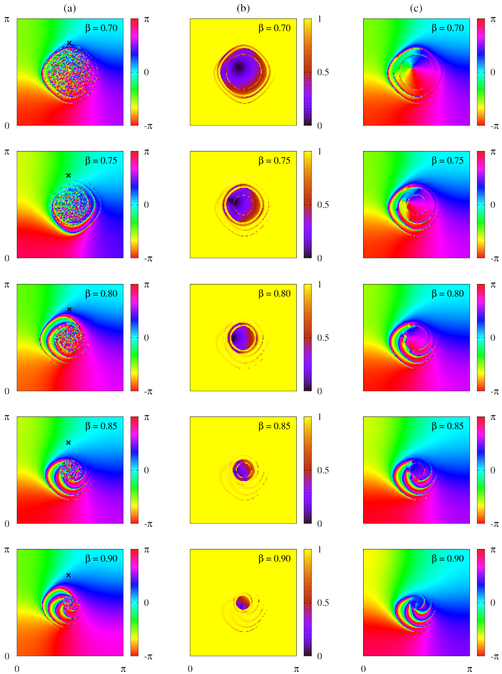

(a)
(b)
(c)
β = 0.70
β = 0.75
β = 0.80
β = 0.85
β = 0.90
π
0
-π
1
0.5

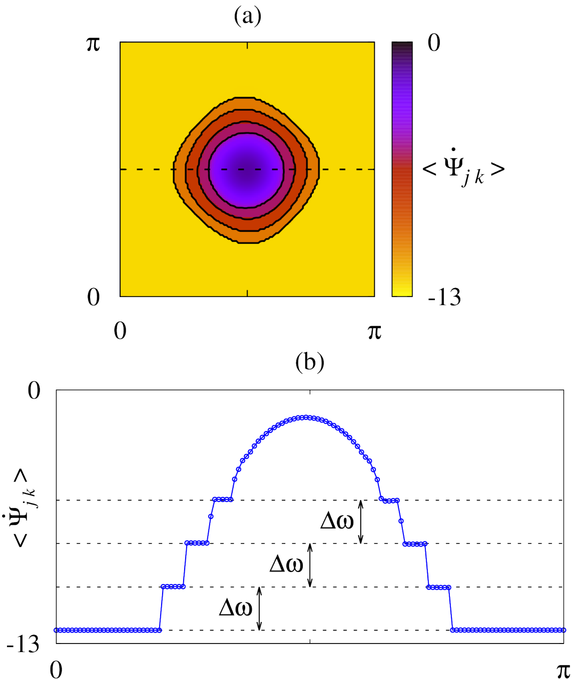
(a)
π
0
0
π
0
-13
$<\dot{\Psi}_{jk}>$
(b)
0
-13
0
π
$<\dot{\Psi}_{jk}>$
Δω
Δω
Δω

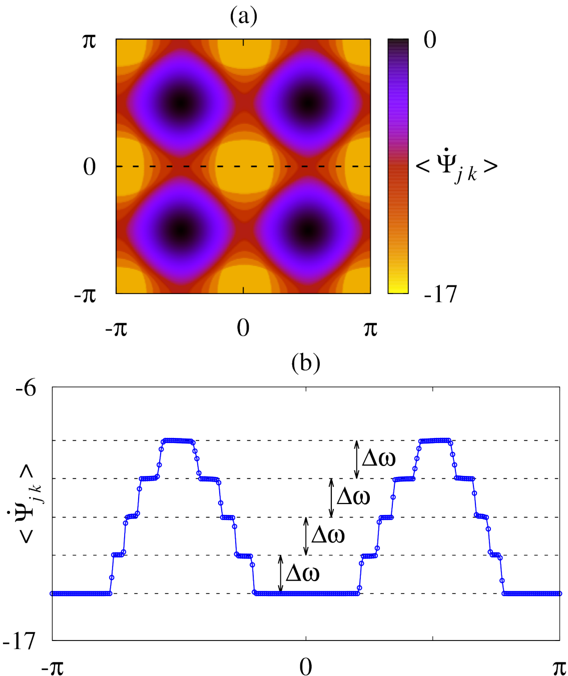

(a)
π
0
-π
-π
0
π
0
$< \dot{\Psi}_{j\,k} >$
-17
(b)
-6
-17
$< \dot{\Psi}_{j\,k} >$
Δω
Δω
Δω
Δω
-π
0
π

# Linear stability of $D_2$ symmetric 4-core chimeras

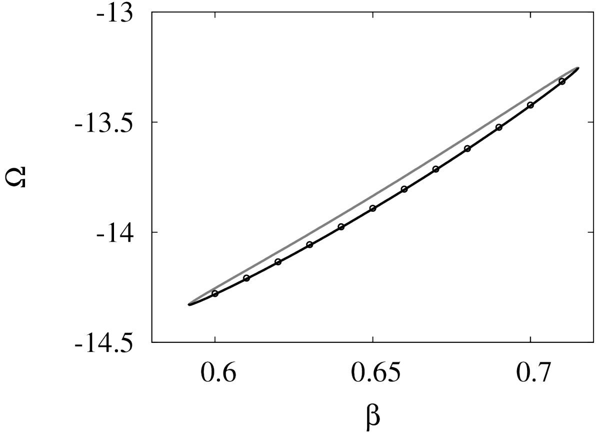


Stable (black) and unstable (gray) parts of an isola of $D_2$-symmetric solutions of the self-consistency equation. Circles show numerical data obtained by dynamical continuation. Parameter: $\gamma = 1.4$.

# Linear stability of $D_4$ symmetric 16-core chimeras

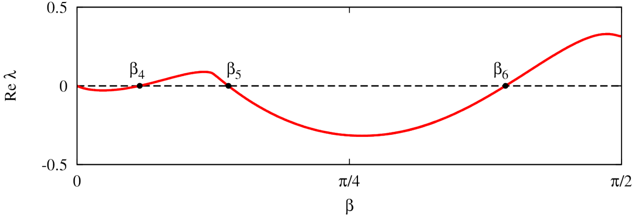


Real part of the eigenvalues when $\gamma = 0.63$. Hopf bifurcation points: $\beta_4 \approx 0.18$, $\beta_5 \approx 0.44$ and $\beta_6 \approx 1.24$.

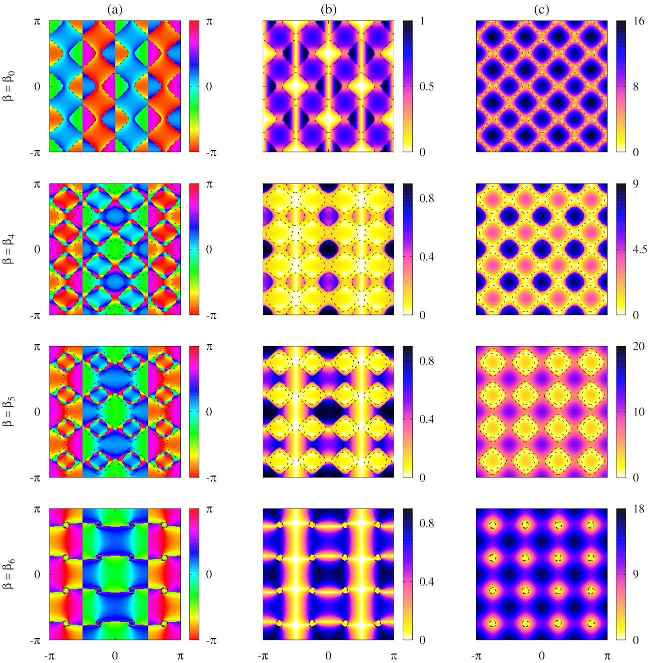

(a)
(b)
(c)
β = β0
β = β4
β = β5
β = β6
π
0
-π
1
0.5
0.8
0.4
16
8
9
4.5
20
10
18

# Conclusion

Several novel states in phase-coupled oscillator systems with nonlocal coupling have been found. These include

- Multi-cluster chimera states
- Traveling (and oscillating) fully coherent states
- Traveling chimera states
- Twisted chimera states
- Multi-core spiral wave chimera states

Many of the properties of these states can be understood by solving the self-consistency relation for these states; the solution of this relation also allowed us to solve the stability problem, and search for bifurcations as the parameter $\beta \equiv \frac{\pi}{2} - \alpha$ varies. The approach extends to systems with spatial inhomogeneity.

## References

J. Xie, E. Knobloch and H.-C. Kao, Phys. Rev. E **90**, 022919 (2014)
J. Xie, H.-C. Kao and E. Knobloch, Phys. Rev. E **91**, 032918 (2015)
J. Xie, E. Knobloch and H.-C. Kao, Phys. Rev. E **92**, 042921 (2015)
O.E. Omel'chenko, M. Wolfrum and E. Knobloch, SIADS **17**, 97–127 (2018)